JGR Atmospheres

RESEARCH ARTICLE
10.1029/2020JD032638

Key Points:
- The performance of ALARO-SURFEX regional climate model is improved by updating the land cover and the Leaf Area Index in Aral Sea region
- Land use/cover change accelerate the warming trend, reduce the summer precipitation and alter the surface energy budget
- The desiccation of Aral Sea induces the most conspicuous influence in regional summer climate

Supporting Information:
- Supporting Information S1

Correspondence to:
G. Luo,
luogp@ms.xjb.ac.cn

Citation:
He, H., Hamdi, R., Cai, P., Luo, G., Ochege, F. U., Zhang, M., et al. (2021). Impacts of historical land use/cover change (1980–2015) on summer climate in the Aral Sea region. *Journal of Geophysical Research: Atmospheres*, *126*, e2020JD032638. https://doi.org/10.1029/2020JD032638

Received 20 FEB 2020
Accepted 16 FEB 2021

Author Contributions:
Data curation: Rafiq Hamdi, Miao Zhang
Formal analysis: Huili He, Rafiq Hamdi, Peng Cai, Friday Uchenna Ochege
Funding acquisition: Geping Luo, Chaofan Li
Methodology: Rafiq Hamdi, Peng Cai, Piet Termonia
Project Administration: Geping Luo
Resources: Rafiq Hamdi, Piet Termonia
Software: Huili He, Rafiq Hamdi, Peng Cai, Piet Termonia
Supervision: Geping Luo, Piet Termonia, Philippe De Maeyer
Validation: Huili He
Writing – original draft: Huili He, Friday Uchenna Ochege

Impacts of Historical Land Use/Cover Change (1980–2015) on Summer Climate in the Aral Sea Region

Huili He[1,2,3], Rafiq Hamdi[1,4,5], Peng Cai[6], Geping Luo[1,2], Friday Uchenna Ochege[1,2], Miao Zhang[7], Piet Termonia[4,5], Philippe De Maeyer[1,3,8,9], and Chaofan Li[10]

[1]State Key Laboratory of Desert and Oasis Ecology, Xinjiang Institute of Ecology and Geography, Chinese Academy of Sciences, Urumqi, China, [2]State Key Laboratory of Desert and Oasis Ecology, University of Chinese Academy of Science, Beijing, China, [3]Department of Geography, Ghent University, Ghent, Belgium, [4]Royal Meteorological Institute, Brussels, Belgium, [5]Department of Physics and Astronomy, Ghent University, Ghent, Belgium, [6]Binjiang College, Nanjing University of Information Science & Technology, Wuxi, China, [7]Northwest Land and Resources Research Center, Shaanxi Normal University, Xi'an, China, [8]Sino-Belgian Joint Laboratory of Geo-information, Urumqi, China, [9]Sino-Belgian Joint Laboratory of Geo-information, Gent, Belgium, [10]Collaborative Innovation Center on Forecast and Evaluation of Meteorological Disaster, School of Geographic Sciences, Nanjing University of Information Science and Technology, Nanjing, China

Abstract In the Aral Sea region, significant land use/cover change (LUCC) occurred in the past 50 years, especially the shrinking of Aral Sea due to unreasonable usage of water resources under intensified agricultural activities. However, to date, regional climatic feedbacks on fine-scale exerted by such LUCC in Central Asia have not been studied clearly. In this study, ALARO-SURFEX regional climate model was used to perform climate simulations under different underlying surface scenarios with 4 km spatial resolution to explore the impacts of historical LUCC on summer climate during 1980–2015. Our results show that compared to default land surface conditions, the modified ones improved the model's ability in simulating temperature, precipitation, and surface energy fluxes. During the period 1980–2015, LUCC accelerated the warming trend, reduced the summer precipitation and altered allocation of surface energy fluxes. Exposed dry bottom of Aral Sea has undergone the most conspicuous warming, which caused increase of the 2 m maximum temperature, average temperature, and diurnal temperature range by 2.56 ± 0.88°C, 1.04 ± 0.53°C, and 3.42 ± 1.10°C, respectively, while minimum temperature decrease by 1.14 ± 0.56°C. The summer precipitation (mainly convective precipitation) decreased by about 2.33 mm overlay the exposed dry bottom of Aral Sea and approximately 400 km "buffer" region in its eastern side. Additionally, the energy balance changed as follows: −47.9, 50.19, −78.67, and −23.72 W m^{-2} for net radiation, sensible heat, latent heat, and soil heat, respectively. Quantified contribution of LUCC on regional climate provides useful information for developing mitigation and adaption strategies under the global warming threat.

1. Introduction

Land surface processes form a dynamic boundary interface within the climate system (Pielke & Niyogi, 2010). Land surface characteristics determine the surface energy balance by assigning the distribution of net radiation into sensible, latent, and ground heat fluxes (Dickinson, 1983). Surface fluxes not only affect temperature and humidity, but also influence wind field and local circulation pattern (Pielke & Niyogi, 2009). Therefore, the land use/cover change (LUCC) is one of the driving forces of the regional and global climate change (Cao et al., 2015; Stocker et al., 2014).

LUCC can affect global and regional climate by means of changing biogeochemistry and biogeophysical properties of terrestrial surface and its associated effect on atmosphere (Kabat et al., 2004). The biogeochemistry effects of LUCC on global climate in terms of greenhouse gas (GHG) emission and carbon assimilation are well studied in the literature (Li, Zhang, et al., 2015; Meinshausen et al., 2009). According to the IPCC AR5, GHG has caused a 0.5–1.3 °C average global surface warming from 1951 to 2012 (Brovkin et al., 2004; Lawrence et al., 2012). However, the climate response to changing biogeophysical properties of terrestrial surface still exits uncertainty, due to regional climate change can be dampened or enhanced by changes in local land surface parameters which depends on the location and the season (Georgescu et al., 2011; Lioubimtseva & Henebry, 2009; Turner, 1988). Several studies examined the climatic impacts of LUCC by

10.1029/2020JD032638

Writing – review & editing: Rafiq Hamdi, Geping Luo, Friday Uchenna Ochege, Miao Zhang, Philippe De Maeyer, Chaofan Li

using general circulation models (GCMs), regional climate models, and observational evidence, they found that the effects on climate are highly regionalized and depend on the LUCC type (Chang et al., 2018; Hua & Chen, 2013; Yamada & Pokhrel, 2019). Especially the arid and semiarid regions, where the summer climate is characterized by a strong interaction between the atmosphere and the land surface, LUCC climate effects could be amplified (Lioubimtseva et al., 2005).

Being one of the driest regions in the world, Central Asia is not only more sensitive to global climate change, but also have been largely affected by regional anthropogenic influence, such as the development of irrigated agricultural (Mirzabaev et al., 2016; Zhang et al., 2019). Especially in Aral Sea region, large irrigation systems were created by the former Soviet Union to divert water from the Amu Darya and Syr Darya rivers in order to promote agriculture production (Lioubimtseva et al., 2005). According to a FAO report, the irrigation of arable land over the Aral Sea basin has increased by 60% from 1962 to 2002, and cotton production has doubled (Yearbook, 2003). Such long-lasting and intense irrigation activities in the Aral Sea basin have modified the underlying surface condition. In fact, the Aral Sea which used to be the world's fourth largest lake in the 1960s, has lost almost 90% of its water surface to date (Roy et al., 2014). Beyond the desiccation of Aral Sea, abandoned and reclaimed farmlands, and grassland degeneration also dramatically changed the land surface characteristics, vegetation and soil features, which might affect the regional climate.

It is accepted that Central Asia is under the threat of dramatic climate change, experiencing the fast warming with the range between 0.27 and 0.47°C in last 50 years (Hu et al., 2014; Ji et al., 2014; Zhang et al., 2016). However, the conclusions based on existing gridded products show large uncertainties in precipitation change. Monthly gridded precipitation from CRU in Central Asia draw a conclusion that increasing trend in summer (2.1 mm decade^{-1}) during late 1970s to 2009 but not significant (Chen et al., 2011), the study based on GPCC draw a similar conclusion but the magnitude is 0.9 mm decade^{-1} (not significant) during 1961–2013 (Song & Bai, 2016). The study based on 240 observations from 1960 to 1991 draw a conclusion that decreasing trend in summer (−1.1 mm decade^{-1}) but not significant (Song & Bai, 2016), while the study based on 75 stations, PRECL, GPCC, and CRU from 1961 to 2013 draw the conclusion that summer precipitation in Central Asia has significantly increased at rate of 3.42, 3.33, 2.67, and 2.43 mm decade^{-1}, respectively (Peng et al., 2019). Those existing work in Central Asia provided the climate change trend, but most of the results came from coarse horizontal resolution gridded data sets and cannot isolate the influence of LUCC (Lioubimtseva et al., 2005; Schiemann et al., 2008).

The regional climate modeling approaches provide a possibility to fill this gap to some extent and are considered as useful tools to separate both the contributions from the intrinsic climate variability and the LUCC to the regional climate with fine-scale resolution. Recent works on regional climate model over Central Asia have focused so far on evaluating the dynamic downscaling methods (Chen et al., 2019; Qiu et al., 2017). Several researches focused on the impact of the shrinking Aral Sea on near-surface temperature, diurnal temperature range (DTR), and precipitation by using regional climate models like WRF and MRCM with spatial resolution of 5–30 km so as to analyze the effects of near-full or idealized fully desiccation of the Aral Sea on regional climate (Mcdermid & Winter 2017; Roy et al., 2014; Rubinshtein et al., 2014; Sharma et al., 2018). However, this region has undergone more complex LUCC during the last 50 years (Chen et al., 2013), such as, abandoned cropland, reclaimed cropland and vegetation degradation. These LUCC may generate an opposite sign to the regional-averaged climate trend (Chen et al., 2017; Pielke et al., 2011). So far, very little information is available on the impact of other LUCC (except for the desiccation of the Aral Sea) on regional climate and their combined effects among the Aral Sea region. Moreover, the coarse spatial resolution may prevent the identification of the effects of different LUCC types. Consequently, large uncertainties still remain concerning the impacts of historical LUCC to observed climate change in the Aral Sea region. Concerted efforts are highly needed to provide climate mitigation and adaption strategies in dealing with warming threat and future development.

Therefore, this study aims to provide a longer period climate change trend with the highest 4 km spatial resolution, and quantifies the impacts of historical LUCC on summer climate in the Aral Sea region from numerical modeling perspective. Specific research objectives are: (1) to evaluate the performance of ALARO-SURFEX regional climate model with default and updated land cover and Leaf Area Index during a decade of simulation from 1980 to 1989; (2) to compute the temperature, precipitation, and surface energy

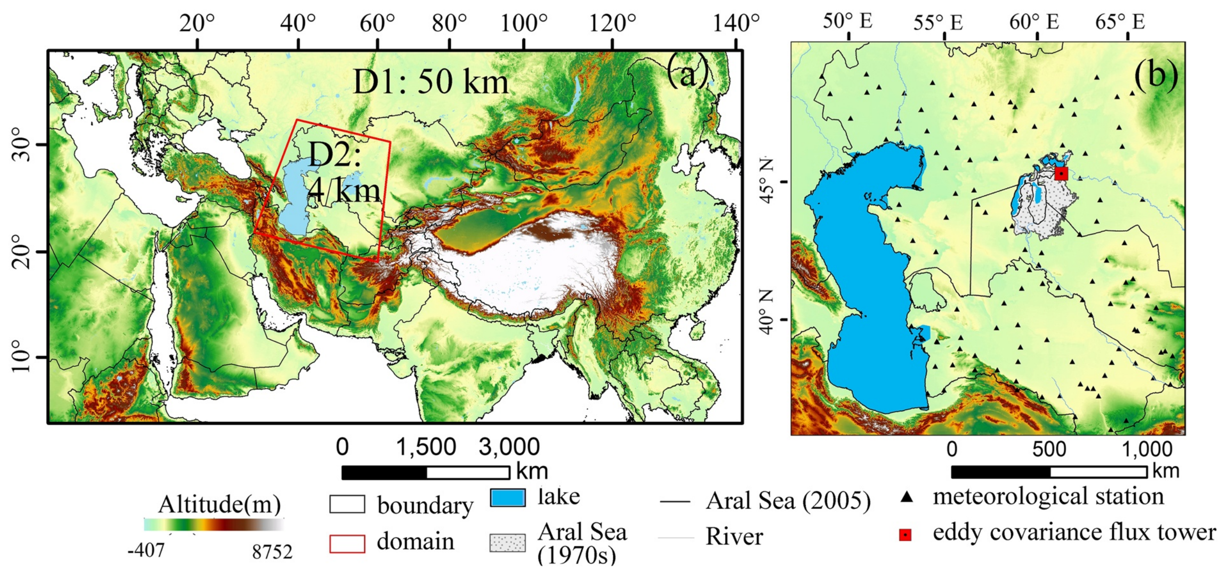

Figure 1. Two-nested modeling domains D1 and D2 with spatial resolution of 50 and 4 km (a), and the locations of the meteorological stations and eddy covariance flux tower (b). The blue fill, black line, and sand-like texture in (b) represent the shoreline of the Aral Sea in 2015, 2005, and 1970s, respectively.

fluxes differences generate by LUCC and their spatial distribution pattern; (3) to quantify the contribution of major LUCC types to regional climate change.

This paper proceeds as follows. Section 2 provides an overview of study area, configuration of the ALARO-SURFEX, data sets used in this study and experimental setup. Section 3 evaluates the model's performance with default and updated land surface condition, and quantifies impacts of historical LUCC in summer temperature, precipitation, and surface fluxes. Section 4 contains the discussion about comparison of our findings with other studies and the limitations in this study. The major conclusions are summarized in section 5.

2. Materials and Methods

2.1. Study Area

The study area covers part of Eurasian continent (Figure 1a). Our region of interest lies within the arid land of Central Asia, from 45.3°E/36.5°N to 67.7°E/48.5°N (Figure 1b). Aral Sea is situated in the center of the domain, dominated by deserts and mountains in the south (Heer, 1993). The Great Caucasus and the world's largest inland water body, the Caspian Sea, forms its western border. The elevation in northern domain is low in west and high in east, from west to east distribute the Caspian lowland, Ustyurt Plateau, and Kazakhskiy Melkosopochnik, respectively. As a terminal lake, water level of the Aral Sea entirely depends on run-off of the Syr Darya and Amu Darya rivers, which start from Pamir and Tian Shan Mountains in the southeastern direction of Aral Sea (Lioubimtseva, 2015). Oases developed along the rivers, where intake water for irrigation were easily available (Shi et al., 2020). Since 1960, the Aral Sea has undergone several stages of desiccation, split into four parts and the water surface area had shrunk by 90%.

2.2. Model Description and Configuration

The regional climate model ALARO version 0 is a new version of the Aire Limitee Adaptation Dynamique Development International (ALADIN) model with an improved physical parameterization to enable simulations at 3–10 km mesh-size (De Troch et al., 2013; Giot et al., 2016; Hamdi et al., 2012; Termonia et al., 2018a, 2018b). This state-of-the-art model has been used at the Royal Meteorological Institute of Belgium for operational numerical weather prediction application since 2010 (Termonia, Fischer, et al., 2018).

The Météo-France SURFace Exteralisee land surface model (SURFEX) provides the key parameterizations to compute the exchange of energy and water between soil, water surface, vegetation, and low-level atmosphere of the regional climate model. The SURFEX is based on a tiling approach to provide information on the surface fluxes according to four types of surface: nature, town, inland water, and sea (Giorgi & Mearns, 1999; Seneviratne et al., 2010). The default land coverage is based on the global ECOCLIMAP II database (Champeaux et al., 2005). SURFEX contains the ISBA (Interaction between Soil, Biosphere, and Atmosphere) scheme for natural surface (Noilhan & Planton, 1989), TEB (Town Energy Balance) scheme for urban surface (Masson, 2000; Masson et al., 2013), FLake scheme for inland water (Salgado & Le Moigne, 2010), and ID TKE (turbulent kinetic energy) oceanic model for sea or ocean (Masson et al., 2013). ISBA includes several submodels simulating the exchanges of energy and water between the soil-vegetation continuums (Le Moigne et al., 2009). TEB is based on the canyon concept, where the town is represented by a roof, a road, and two facing walls (Le Moigne et al., 2009). The one-dimensional oceanic model described by Gasper (Gaspar et al., 1990) which allows to represent the oceanic vertical mixing according to a parameterization from Bougeault and Lacarrere adapted to grid point containing a fraction of sea (Bougeault & Lacarrere, 1989).

SURFEX allows for exchanges between the surface and the atmosphere through a standardized interface (Best et al., 2004), which leads to the possibility of running it either in offline mode or with coupling to atmospheric model ALARO (Le Moigne et al., 2009). The regional climate model ALARO-SURFEX has been validated for a climate simulation and proved reliable to represent the regional climate and land surface process in Europe (Berckmans et al., 2017; Hamdi et al., 2014) and northwestern China (Cai et al., 2020).

The regional climate model was driven by ERA-Interim reanalysis data set with spatial resolution of $0.75° \times 0.75°$ (Dee et al., 2011). This study utilizes the Free Surface downscaling approach (Berckmans et al., 2017), which reinitialized the atmosphere daily and simulated the land surface continuously with a single initialization (Giorgi & Mearns, 1999). To be specific, the zonal and meridional wind components, atmospheric temperature, specific humidity and surface pressure were updated in every 6 h by forcing data, while the soil moisture and soil temperature was initialized only once in the start of the simulations. It allowed the model to simulate the atmospheric fields close to the reanalysis forcing, while the land surface conditions were kept continuous by adding the land surface conditions of previous daily simulation. The sea surface temperature was updated daily in order to employ all possible data. With this downscaling approach, land surface spin-up lasted for 3 months, which was sufficient for the soil parameters (especially deep soil moisture) to get to the equilibrium state.

2.3. Mapping of the Land Surface Condition

The ECOCLIMAP II database provides both land cover data at 1/120° spatial resolution and its corresponding land surface parameters and soil texture (Jahn et al., 2006) as input for SURFEX. ECOCLIMAP II classifies the globe into 573 ecosystems, which is obtained by combining the existing land cover (GLC2000 and CLC2000) with climate maps (Champeaux et al., 2005; Faroux et al., 2013) as shown in Figure 2a. The biophysical parameter Leaf Area Index (LAI) is initialized on the land cover level from lookup tables with the annual cycle of LAI stemming from the MODIS LAI from January 2002 to December 2006 (Faroux et al., 2013). Due to the use of outdated land cover maps, the ECOCLIMAP II failed to correctly represent land cover status of Central Asia by underestimating the area of anthropic zones compared to results of a multisource land cover data set (Chen et al., 2013). Therefore, the ECOCLIMAP II covering the region of Central Asia has been updated by independent local data generated by the Xinjiang Institute of Ecology and Geography, Chinese Academy of Sciences (abbreviated as XIEG-LUC) (Chen et al., 2015). The XIEG-LUC was derived from the Landsat satellite images and passed the accuracy check. It contains three periods of land use/land cover map the 1970s, 2005, and 2015 as shown in Figures 2b–2d.

Among them, Inland water includes: lake and subpolar wetland. Forest includes: boreal evergreen needle leaf forest, Asia tropical evergreen broad leaf forest, Asian boreal deciduous needle leaf forest, North Hemisphere (NH) continental mixed forest and Asia wet tropical wood land. Close Shrub includes: Asia continental close shrub, Asia polar closed shrub and Asia tropical close shrub. Open Shrub includes: NH arid open shrub, Asia dry tropical open shrub and NH polar open shrub. Grass land includes: NH semiarid continental grass, NH subpolar wood grass, NH continental wood grass and Asia wet, bare soil with spare

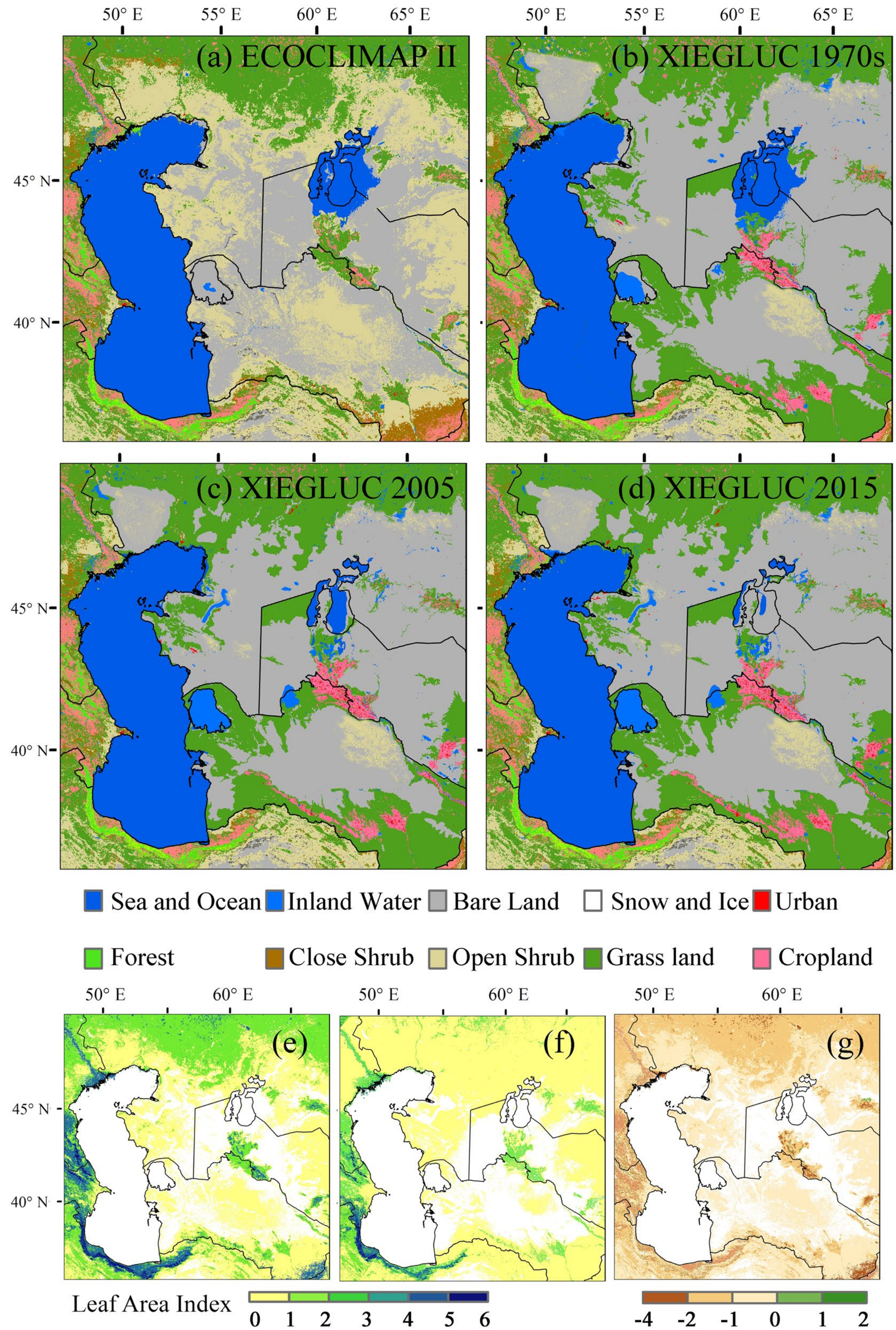

Figure 2. (a) The default land cover map from ECOCLIMAP II and land cover maps in (b) 1970s, (c) 2005, and (d) 2015 generated by XIEG. The default (e) and updated (f) Leaf Area Index values are also shown, along with their difference (default—updated) (g).

Table 1
Major LUCC and Their Percentage in Total Area Which Went Through LUCC in the Aral Sea Region

1970s to 2005		1970s to 2015	
Categories	Percentage	Categories	Percentage
Lake to bareland	21.00%	Bareland to grassland	24.26%
Cropland to grassland	19.51%	Lake to bareland	20.78%
Bareland to grasslands	15.08%	Cropland to grassland	19.08%
Bareland to water body	13.80%	Grassland to bareland	9.66%
Grassland to cropland	10.13%	Grassland to cropland	8.94%

polar vegetation and dry tropical wood grass. Cropland includes: irrigation crops, Asia semiarid continental crops, Asia humid continental crops, Asia polar crops, warm temperate crops and rice field.

The implementation procedure of the updated land cover conditions and LAI according to these three steps: (1) converting the land cover types from XIEG-LUC to ECOCLIMAP II. (2) resampling the XIEG-LUC to match the 1/120° horizontal resolution. (3) recalculating LAI in Aral Sea region, and updating the lookup table.

First, the ECOCLIMAP II and the XIEG-LUC made by different land use/cover classification systems. The XIEG-LUC adopted the Chinese Land Use Classification System, which only had a brief description on the vegetation function type (Chen & Zhou, 2007). Therefore, we converted the XIEG-LUC into the ECOCLIMAP II system by referring the vegetation fraction type of typical vegetation in Central Asia collected from previous research (Zhang et al., 2016). The conversion rules are summarized in Table S1 in the supplemental material.

Second, the original shapefile format of the XIEG-LUC data set was converted into a raster format with spatial resolution of 1/120° by selecting the most abundant land cover type inside each grid.

Third, we updated the LAI value in the lookup table by calculating the LAI values of 30 land cover types presented in the 2005 map of XIEG-LUC. Specifically, we computed LAI value of each grid over the Aral Sea region using the mean values of MOD15A2H from 2004 to 2013 (Yan et al., 2016). Then we took each land cover type as mask to extract their corresponding grids in the LAI maps and computed the grids' mean value. Finally, we updated the lookup table by the new LAI values of each land cover type.

2.4. General Trends in the Historical LUCC

We computed and showed the percentage of each types of LUCC on the total area that experienced LUCC in Table 1. The major LUCC in our study area were the bidirectional conversion between the (1) inland water (hereafter referred to as lake) and bareland, (2) bareland and Asia semiarid continental grassland (hereafter referred to as grassland), (3) cropland and grassland.

The characteristics of the LUCC were triggered by both natural and anthropogenic influence. Natural vegetation is sensitive to precipitation, which cause the change of bareland and grassland (Li, Chen, et al., 2015; Seddon et al., 2016). Large amount of water withdrawn from rivers caused the shrinking of the Aral Sea, while excess irrigation discharged into lowland formed new lakes, like Sarygamysh lake or coastal evolution based expansion of water area (Gaybullaev & Chen, 2012; Yang et al., 2019). The collapse of the Soviet Union led to cropland abandonment, although has been reclaimed after 2000. The total cropland area in 2015 still less than in 1970s (Chen et al., 2015).

2.5. Experimental Design

In this study, we run the ALARO-SURFEX regional climate model on two-nested domains. A domain with spatial resolution of 50 km and 169 × 117 grid boxes covers part of Eurasian continent to give lateral boundary condition for the nested domain within the outer domain at spatial resolution of 4 km with 500 × 500

Table 2
Numerical Experiments Set-Up

Experiments		LBC	Land surface	LAI
Validation	Case 1	1980–1989 JJA	Default	Default
	Case 2	1980–1989 JJA	XIEG-LUC 1970s	Updated
Analyzing	Case 3	1980–2015 JJA	XIEG-LUC 1970s	Updated
	Case 4	1980–1995 JJA	XIEG-LUC 1970s	Updated
		1996–2008 JJA	XIEG-LUC 2005	Updated
		2009–2015 JJA	XIEG-LUC 2015	Updated

grid boxes. The domain is vertically divided into 46 layers, separated by hybrid pressure terrain-following levels, and the height of the lower layer is about 17 m above ground (Simmons & Burridge, 1981). The model time step is 450 and 180 s for 50 and 4 km domain, respectively. Two groups of numerical simulation have been conducted (as summarized in Table 2). The first group of experiments was used to evaluate the impact of the land surface condition on the performance of ALARO-SURFEX. The second group of experiments was utilized to analyze the contribution of historical LUCC on the summer climate.

The first group of simulations covered a 10-summer (June-July-August) period from 00:00 UTC on June 1 to 24:00 UTC on 31 August during the period of 1980–1989 when more meteorological stations were available. Although the 10-summer length is arbitrary, it is sufficient to generate a reasonable sample to evaluate the sensitivity of the model to the different land cover conditions. In the first 10-summer simulation group, Case 1 (see Table 2) applied used the default ECOCLIMAP II data set and its corresponding LAI, while Case 2 used the data set of the XIEG-LUC 1970s and updated LAI profile.

We conducted the second group of simulations for a longer period, covering 36-summer period from 1980 to 2015 with identical meteorological boundary conditions but with a varying land cover status (see Table 2). The land cover condition of Case 3 was kept constant (using the land cover status in XIEG-LUC 1970s) during the simulation period from 1980 to 2015. Due to the limitation of the land cover maps provided by the XIEG, in Case 4 we used land cover conditions in1970s, 2005, and 2015 to represent the land cover condition of the following period 1980–1995, 1996–2008, 2009–2015, respectively.

2.6. Observational Reference Data

The meteorological stations collected from the Global Historical Climatology Network were used to validate the simulation results for 2 m temperature and daily precipitation (Menne et al., 2011). All selected stations data were subjected to quality control, and only the stations showing less than 20% missing values were selected (Peterson et al., 2015). There are 125 gauges within the innermost domain which contained the daily precipitation, while 97 stations contained temperature values.

The Eddy Covariance system was installed in April 2012, located on a desert grassland at 61.08°N 45.96°E, 23 km from the nearest coast of the Aral Sea. It is surrounded by desert, irrigation farmland, and shrubland. Half-hourly fluxes of net radiation (RN), ground heat (G), sensible heat (H), and latent heat (LE) observed from June 1 to August 18, 2012 have been used in this study (Ochege et al., 2019). Furthermore, the net radiation flux is defined as the sum of the observed net shortwave and longwave radiation fluxes.

2.7. Evaluation Metrics

We used several statistical measures for the evaluation of 2 m temperature and surface energy fluxes, including root mean square error (RMSE), coefficient of determination (R^2), and trend line of the coefficient, in order to comprehensively evaluate the simulation results. Those measures describe the direction of error bias, and also indicate the average error magnitude:

$$\mathrm{MBE} = \frac{1}{N}\sum_{i=1}^{N}\left(M_i - O_i\right)$$

$$\mathrm{RMSE} = \sqrt{\frac{1}{N}\sum_{i=1}^{N}\left(M_i - O_i\right)^2}$$

$$R^2 = \left(\frac{\sum_{i=1}^{N} \left(M_i - \bar{M}\right)\left(O_i - \bar{O}\right)}{\sqrt{\sum_{i=1}^{N} \left(M_i - \bar{M}\right)^2} \sqrt{\sum_{i=1}^{N} \left(O_i - \bar{O}\right)^2}} \right)^2$$

where N is the total number of comparisons, M is the modeled value, and O is the stations' observation value and $\bar{M} = \frac{1}{N}\sum_{i=1}^{N} M_i$, $\bar{O} = \frac{1}{N}\sum_{i=1}^{N} O_i$.

Due to the dry summer climate characteristics in this region, we used the Perkins' skill score (PSS) (Perkins et al., 2007) to evaluate the ALARO-SURFEX performance of simulated daily precipitation. This metric computes the cumulative minimum value of two distributions of each binned value (1 mm). If a model simulates the observed conditions perfectly, the skill score will be equal to one, which is the total sum of the probability at each bin center in a given frequency. Expressed formally,

$$S_{score} = \sum_{1}^{n} minimum\left(Z_m, Z_o\right)$$

where n is the number of bins employed to calculate the frequency distribution, Z_m and Z_o represent the frequency of the values in a given bin from the model and observed data. This provides a comparable measure of relative similarity between the model and the observed frequency.

3. Results

3.1. Evaluation of the ALARO-SURFEX in the Aral Sea Region

3.1.1. 2 m Temperature

The simulation results of the default (Case 1) and updated (Case 2) land surface conditions were compared to the observations (OBS) for daily maximum (T2max), average (T2avg), and minimum (T2min) 2 m temperature in each station as shown in Figures 3a, 3c, and 3e. Considering the potential influence of water bodies, we further divided the stations into two groups according to their distances (<200 km) to the Aral Sea and Caspian Sea (Small, Sloan, & Nychka, 2001). We performed t test on the observations around and far from water bodies. The T2max difference between the two groups is significant (p value < 0.05), while T2avg and T2min differences are not significant. Case 2 has similar conclusion, but Case 1 shows that T2max and T2avg difference is not significant, T2min difference is significant.

In order to summarize how closely the two Cases match with observations, we adopted the Taylor diagram to show their values of correlation coefficient and root mean square under different Cases and whether around water bodies in Figures 3b, 3d, and 3f. Temporal distribution of the mean value of T2max, T2avg, and T2min are shown in Figure 3g. The results indicate that the performance of Case 2 is better than Case 1 in describing the daily temperature. RMSE of T2max in Cases 1 and 2 have similar magnitude with values of 3.16°C and 3.03°C, respectively. RMSE of T2avg in Case 1 is 2.98°C larger than in Case 2 (1.88°C). Case 2 also has better ability in simulating T2min, RMSE of Case 1 and 2 are 3.38°C and 1.78°C, respectively.

Based on the conclusion that the performance of Case 2 is better, we focus on the results of Case 2 in describing the influence of water bodies on performance of ALARO-SURFEX. The stations around water bodies show smaller RMSE (T2max: 3.06°C T2avg: 1.59°C, T2min: 1.59°C) than the other stations (T2max: 3.09°C, T2avg: 2.10°C, T2min: 1.94°C). However, the stations around water bodies show lower R^2 (T2max: 0.64, T2avg: 0.71) than the other stations (T2max: 0.84, T2avg: 0.78), the R^2 of T2min (0.57) is similar in both station groups.

Although deficiencies still exist, both simulations underestimate the temperature, the model with updated land surface conditions largely corrects the RMSE and R^2. The magnitude of RMSE in T2max tends to be larger than T2min and T2avg, indicating that the simulation of the maximum temperature is more challenging during the summer period in the Aral Sea region.

10.1029/2020JD032638

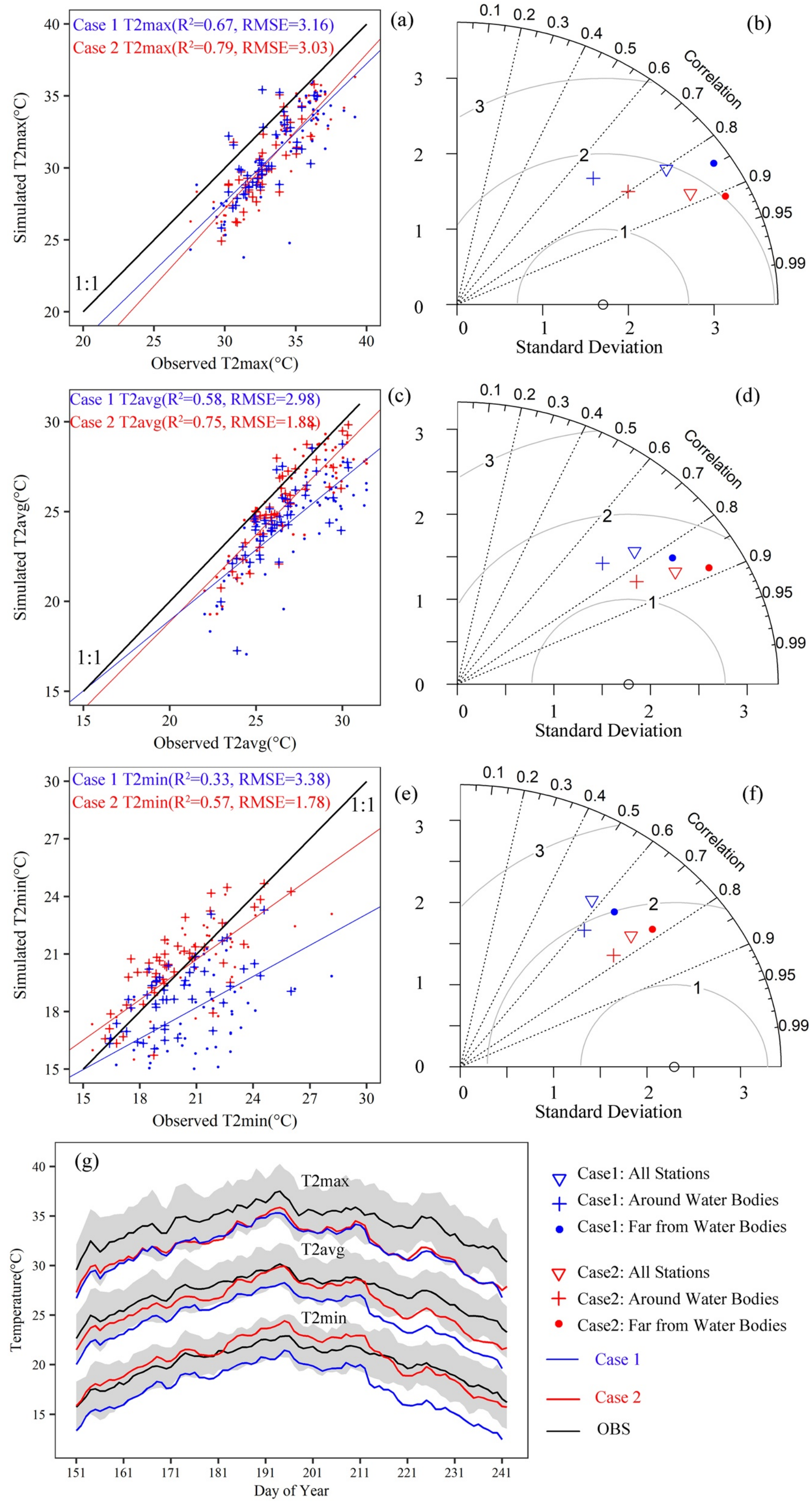

Figure 3. Evaluating the performance of ALARO-SURFEX in simulating 2 m temperature under different underlying land surface scenarios. Scatter diagrams of (a) T2max, (c) T2avg, (e) T2min, and their temporal distribution during summer (g) are in the left panel. Taylor diagrams of simulated T2max (b), T2avg (d), and T2min (f) with different groups of stations are in right panel. The shade in (g) represents ± one standard deviation for OBS.

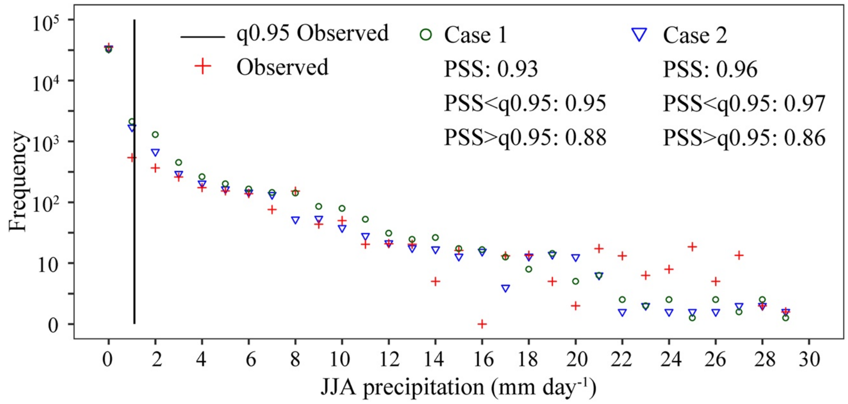

Figure 4. Evaluating the performance of ALARO-SURFEX in simulating frequency distribution of the JJA daily precipitation amount under different underlying land surface scenarios. The Perkins' skill score is shown for all values, including values that are lower than the 95th percentile (in the left of vertical line), and values higher than the 95th percentile (in the right of vertical line).

3.1.2. Precipitation

According to the Köppen climate classification system, Uzbekistan, Turkmenistan, and south Kazakhstan are characterized as arid and dry summer climate (He et al., 2021). Therefore, the 95th percentile of the precipitation events amounted to less than 1 mm day^{-1}. We defined the rainy days by taking into account the daily precipitation above 0.1 mm day^{-1} (because this amount might be important in arid regions) (Qiu et al., 2017). Any daily rainfall in each grid is considered as an event. We present the frequency distribution for all precipitation events based on Case 1 and Case 2 against observations in Figure 4. The result shows that the summer precipitation is well represented by both simulations. The simulation with default land cover condition (Case 1) is less accurate on simulating the daily precipitation (especially the small amounts of precipitation), but with a better ability to simulate large precipitation amount in summer than Case 2. This is confirmed by the PSS, which stands a measure of similarity between two distributions. The PSS scores are 0.95 and 0.97 for Cases 1 and 2 in precipitation values lower than 95th percentile (vertical line), respectively, but measured 0.88 and 0.86 in precipitation values higher than 95th percentile, respectively. It is worth noting that in the upper tail of the distribution (above 20 mm day^{-1}), both simulations are less close to the observation, indicating that an accurate simulation of the extreme precipitation event is challenging.

3.1.3. Surface Energy Fluxes

Figure 5 shows the performance of the ALARO-SURFEX in simulating surface energy fluxes based on the setup of Case 1 and Case 2. Both Cases could capture the hourly pattern of net radiation (Figure 5a), and their R^2 are both larger than 0.93 ($p < 0.01$) (Figure 5b). The updated model shows better ability to simulate the RN in regard to R^2 and RMSE, despite the model simulation and observation exits discrepancies during daytime from 10:00 to 16:00 local time.

A strong linear relationship is found between the simulations and observations for sensible heat (Figures 5c and 5d) and with R^2 of 0.84 in Case 1 and 0.87 in Case 2. However, both simulations overestimated H between 10:00 and 20:00 local time. Case 1 presents a higher R^2 but the MBE value (62.39 W m^{-2}) almost doubled than in Case 2 (32.18 W m^{-2}).

In contrast to the sensible heat, both Cases underestimated the latent heat in diurnal as shown in Figures 5e and 5f. The MBE of the Case 2 (−17.34 W m^{-2}) is smaller than in Case 1 (−28.94 W m^{-2}). The difference of LE and H between Cases 1 and 2 may explain by the different underlying surface conditions around EC station. The EC station is covered by semiarid continental grassland with LAI value of 0.67 (mean value during the summer) in Case 2, while land cover type in Case 1 is bareland with LAI value of 0.

In the arid region, ground heat usually represents the smallest amount among all energy flux components. Both Cases showed a peak value that occurred more than 2 h earlier than in the observation. As

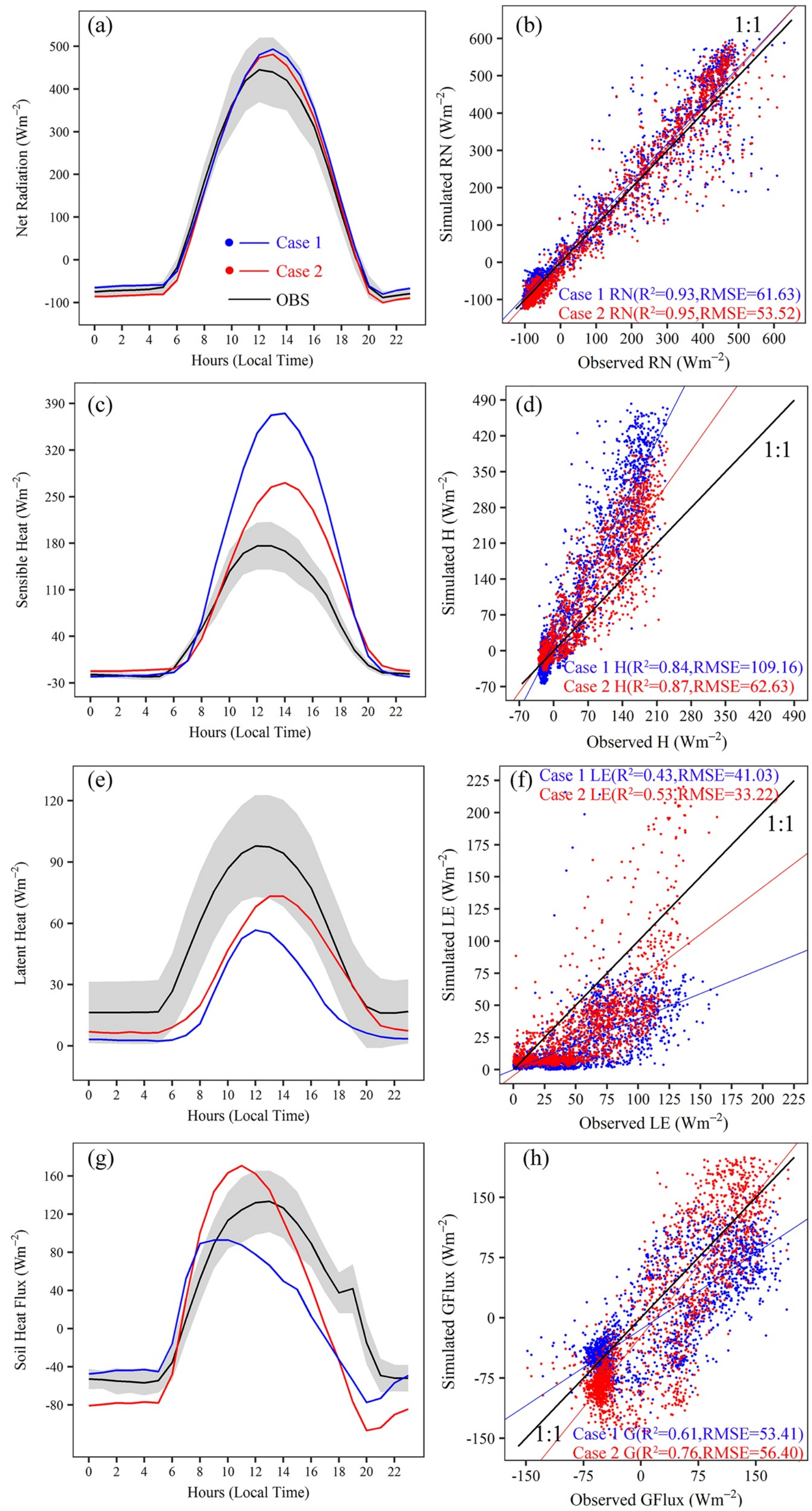

Figure 5. Evaluating the performance of ALARO-SURFEX in simulating surface energy fluxes under different underlying land surface scenarios. Diurnal variation comparison of net radiation (a), sensible heat (c), latent heat (e), and ground heat (g) in left panel and corresponding scatter diagram (b, d, g, h) on the right panel. The shade in left panel represents ± one standard deviation from OBS.

demonstrated in Figures 5g and 5h, the R^2 are 0.76 and 0.61, MBE are −18.58 W m^{-2} and −23.49 W m^{-2}, RMSE are 53.41 W m^{-2} and 56.40 W m^{-2} in Cases 1 and 2, respectively.

These results indicate that more realistic representation of land surface condition could improve the performance of ALARO-SURFEX in simulating temperature, precipitation, and surface energy fluxes. Therefore, the land cover maps generated by XIEG and updated LAI profile are adopted for following analysis.

3.2. Impacts of the Historical LUCC on Summer Climate

3.2.1. 2 m Temperature

With the limitation of the XIEG-LUC data set available, we kept land cover status in 1970s during 1980–2015 in Case 3, while we altered the land cover status two more times in Case 4. Consequently, the temperature difference is computed from Case 4 to Case 3 (using their 36-summer mean value) shows comprehensive LUCC impacts during 1980–2015. In this section, we used the student-test to calculate the significance of LUCC effects on each grid and only the grid significant at 1% level (p value < 0.01) was selected in following statistics. The spatial distribution of temperature difference generated by LUCC is in the range of −8°C to 6°C as demonstrated in Figures 6a–6c. Temperature in Case 4 is higher than in Case 3 in the regions of Caspian lowland desert, Ustyurt Plateau, exposed dry bottom of Aral Sea, oasis, and cities along the rivers. Temperature in Case 4 is lower than in Case 3 regarding the newly expanded water surface.

Regarding to the domain average, LUCC induced T2max and T2avg to increase with approx. 0.17 and 0.12°C, and T2min to decrease by 0.10°C. The most noticeable and larger amount of temperature differences are triggered by the bidirectional conversion between the land and water surface. Due to the fact that land surface absorbs and releases heat quicker than water surface, spatial pattern of the T2max difference is opposite to T2min over the region that experienced conversions between the lake and bareland. Therefore, the disappearing Aral Sea has induced warming effect on T2max and T2avg with magnitude of 2.56 ± 0.88 and 1.04 ± 0.53°C and a cooling influence on T2min with a magnitude of 1.14 ± 0.56°C. The impact of desiccation of Aral Sea in T2avg was not only confined in the region of exposed dry bottom of Aral Sea, but ~400, ~310, ~170 km away on its eastern, southern, and western side, respectively. The newly formed water surface shows an inverse impact on the surrounding temperature with a similar magnitude (but their "buffer" region was confined within 100 km).

LUCC also triggered a change in DTR. The spatial distribution of DTR difference (as showed in Figure 6d) demonstrates that LUCC caused DTR to enlarge in the Aral Sea and its immediate surrounding (less than 50 km) and southern Turkmenistan. The south of Aral Sea, the Aktobe region and the newly formed water surface shows a smaller DTR in Case 4 than in Case 3. Regarding to domain average, LUCC induces 0.10°C increasing of DTR. The exposed dry bottom of Aral Sea causes DTR increasing with a magnitude of 3.42 ± 1.10°C, the newly formed water surface narrows DTR by 2.35 ± 1.68°C.

In order to split the global climate change which contains in forcing data and climate change induced by LUCC, we used linear regression analysis significant at 1% level to calculate the temperature change rate in both simulations. The temperature change rate of Case 3 will represent the trend of background temperature change, due to the fixed land surface condition. The temperature change rate of Case 4 significant at 1% level represents the simultaneous effects of background climate change and LUCC. Therefore, the temperature change rate difference (computed from Case 4 to Case 3) could be defined as the climate change induced by LUCC. To quantify the impacts of each LUCC type on temperature, we divided the period into two part according to their land cover conditions. The temperature change rate in Cases 4 and 3 significant at the 1% level during 1980–2008 and 1980–2015 (refer to two period in following) were employed to assess contribution of LUCC on temperature.

In both periods, the background temperature shows a warming trend. The rate is in the range of 0.35–0.49°C decade^{-1} over land surface, while over the water surface is in the range of 0.14–0.17°C decade^{-1}. However, the temperature change rates response to different LUCC types vary in magnitudes and direction as shown in Table 3. Conversions from lake to bareland, from cropland to grassland and from grassland to bareland accelerate the warming trend. The conversions from bareland to grassland, from grassland to cropland and the newly formed water surface mitigate the warming trend. Among them, the shrinking Aral

10.1029/2020JD032638

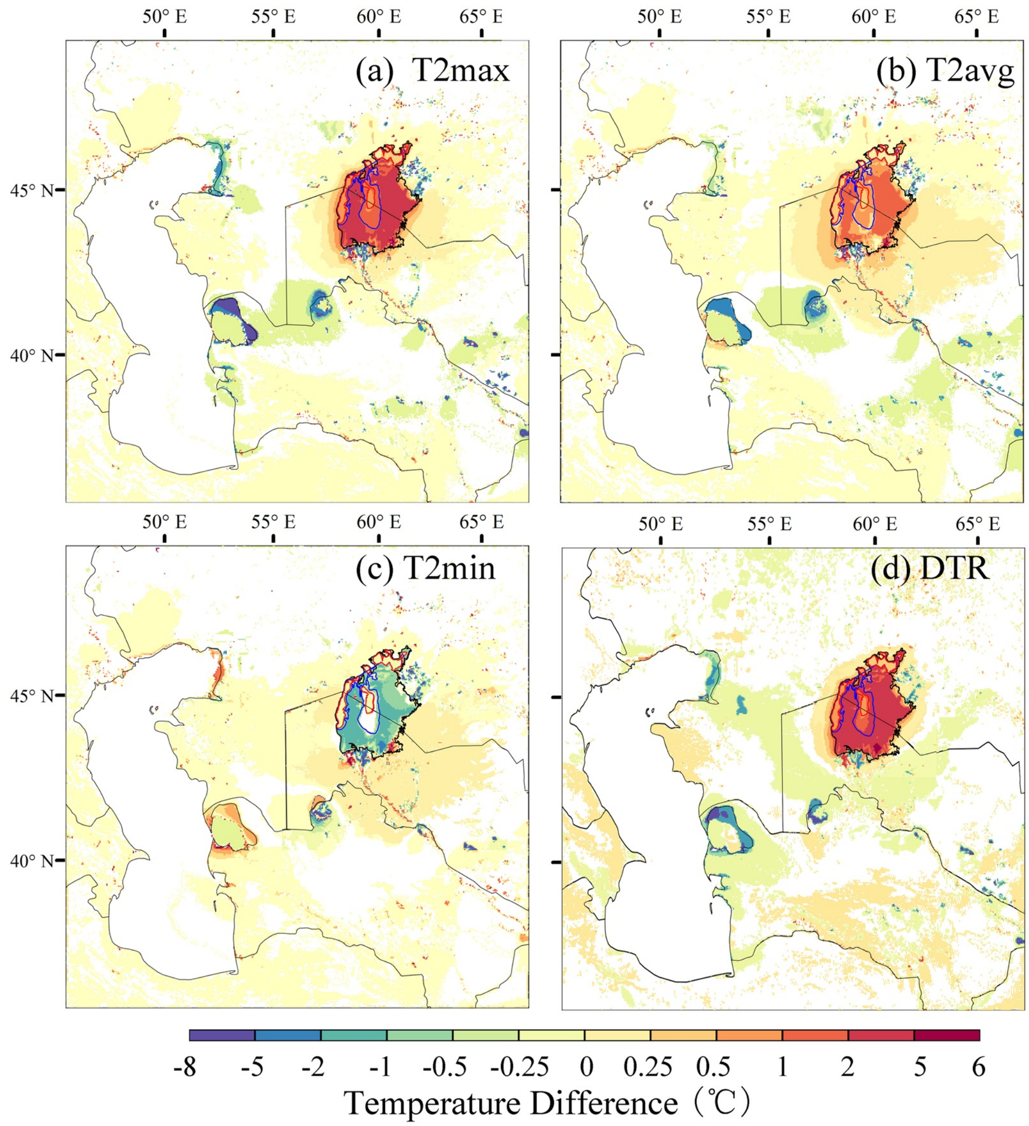

Figure 6. The spatial distribution of T2max (a), T2avg (b), T2min (c), and DTR (d) differences computed from Case 4 to Case 3 with mean value of 36-summer.

Sea generates most conspicuous and strongest impact in both periods. The exposed dry bottom of the Aral Sea accelerates T2max (T2avg) warming trend with approximately 1.00°C (0.46°C) decade^{-1} and 1.07°C (0.49°C) decade^{-1} during 1980–2008 and 1980–2015, respectively. Meanwhile T2min shows an opposite sign in the background trend, with a cooling effect about 0.36 and 0.37°C decade^{-1} in two periods, respectively, which naturally amplifies the DTR with magnitude of 1.23 and 1.30°C decade^{-1}. Abandoned cropland slightly causes acceleration in the warming trend in T2avg with magnitudes of 0.08°C and 0.09°C decade^{-1}, and enlarges DTR with 0.11°C and 0.14°C decade^{-1} in the two periods, respectively. Vegetation restoration slightly mitigates the warming trend about 0.09°C and 0.06°C decade^{-1} and decreases the DTR by approximately 0.12 and 0.11°C decade^{-1} in the two periods, respectively. The newly formed water surface shows opposite sign with background trend of T2max and T2avg by 0.74 and 0.42°C decade^{-1}, increases T2min's trend by 0.34°C decadal^{-1}, and decreases DTR with a rate amount to 1.09°C decade^{-1} during 1980–2008. Reclaimed farmland from grassland slightly mitigates the T2avg warming trend by 0.05°C decade^{-1} in both periods.

Table 3

Comparison of the Decadal Temperature Change Rate (°C decade^{-1}) Significant at 1% Level Over Grid Cells Associated With Major LUCC Type Between the 1970s and 2005, 1970s and 2015, and Background Temperature Change Rate in the Corresponding Grid Cells

		Temperature change rate induced by LUCC (°C decade^{-1})				Background temperature change rate(°C decade^{-1})			
Period	Types	T2max	T2avg	T2min	DTR	T2max	T2avg	T2min	DTR
LUCC between the 1970s and 2005	Lake to Bare land	1.00	0.46	−0.36	1.23	0.17	0.16	0.15	0.10
	Cropland to Grassland	0.08	0.03	−0.05	0.11	0.43	0.45	0.48	−0.04
	Bareland to Grassland	−0.09	−0.03	0.05	−0.12	0.48	0.43	0.45	0.15
	Bareland to Water Body	−0.74	−0.42	0.34	−1.09	0.38	0.36	0.35	0.15
	Grassland to Cropland	−0.06	−0.05	0.03	−0.12	0.42	0.38	0.36	0.15
LUCC between the 1970s and 2015	Bareland to Grassland	−0.06	−0.03	0.04	−0.11	0.48	0.44	0.39	0.12
	Lake to Bareland	1.07	0.49	−0.37	1.30	0.16	0.15	0.14	0.10
	Cropland to Grassland	0.09	0.06	−0.04	0.14	0.47	0.45	0.40	0.10
	Grassland to Bareland	0.08	0.05	−0.04	0.03	0.49	0.44	0.44	0.17
	Grassland to Cropland	−0.07	−0.05	0.03	−0.08	0.42	0.39	0.37	0.22

The background temperature change rate was computed from the trend of Case 3 without the LUCC influence. The LUCC contributions in temperature change rate were computed from trend of Case 4 to trend of Case 3.

3.2.2. Precipitation

Figure 7a presents the summer precipitation difference computed from Case 4 to Case 3. In spatial pattern, LUCC induces a reduction of total summer precipitation in eastern side of Aral Sea. In order to better understand the impacts of the historical LUCC on precipitation magnitude, we regarded the daily precipitation in each grid as a rainfall event, then compared the distribution of rainfall event frequency in each magnitude (based on Cases 3 and 4). The results indicate that the number of days without precipitation (0 mm) in Case 4 is greater than in Case 3, but in other magnitude of precipitation Case 4 is less than Case 3 (not shown), which means that LUCC induces a summer drought intensification in this region.

The impacts of desiccated Aral Sea in summer precipitation are not symmetrically confined to the immediate vicinity of the Aral Sea area. On the eastern side of Aral Sea, summer rainfall of Case 4 is 2.33 mm less than in Case 3. To further explore the summer precipitation response to the shrinking Aral Sea, we computed the convective precipitation and large-scale precipitation difference between Cases 3 and 4, the convective precipitation shows a similar spatial distribution to the total precipitation and accounted for 88% of the total precipitation change. The range of influence extends to approximately 400 km in the eastern Aral Sea, which might be understood by considering the local circulation pattern.

We plotted the hourly 10 m wind direction and wind speed over the grids that showed significantly difference of total precipitation in the eastern Aral Sea. The prevailing wind direction in both simulations includes the north-northeast wind (NNE), northeast wind (NE), and east-northeast wind (ENE). The desiccation of Aral Sea causes decreasing in frequency of the north (N), NNE, south (S), south-southwest (SSW), southwest (SW), and west-southwest (WSW) wind, while the frequency of wind direction in northeast (NE), ENE, and east (E) are increased. The average wind speed in Case 4 was lower than in Case 3 about 0.39 m s^{-1}. The lost water surface weakens the circulation between the Aral Sea and surrounding desert, especially the reduction in SW wind that crosses Aral Sea with moist air.

3.2.3. Surface Energy Fluxes

In this study, we analyzed the impacts of LUCC on the summer surface energy fluxes containing the net radiation, sensible heat, latent heat, and ground heat flux. As illustrated in Figure 8a, in spatial distribution, RN in Case 4 is higher than in Case 3 in the Caspian lowland, Sarygamysh Lake, Garabogazköl, and oasis along the rivers, but lower than in Case 3 in the dry-up Aral Sea. The H difference shows an opposite pattern in the above regions (but not significant in Caspian lowland) in Figure 8b. The spatial distribution of LE difference between Cases 4 and 3 is similar to net radiation but the impact is limited to a smaller region seen

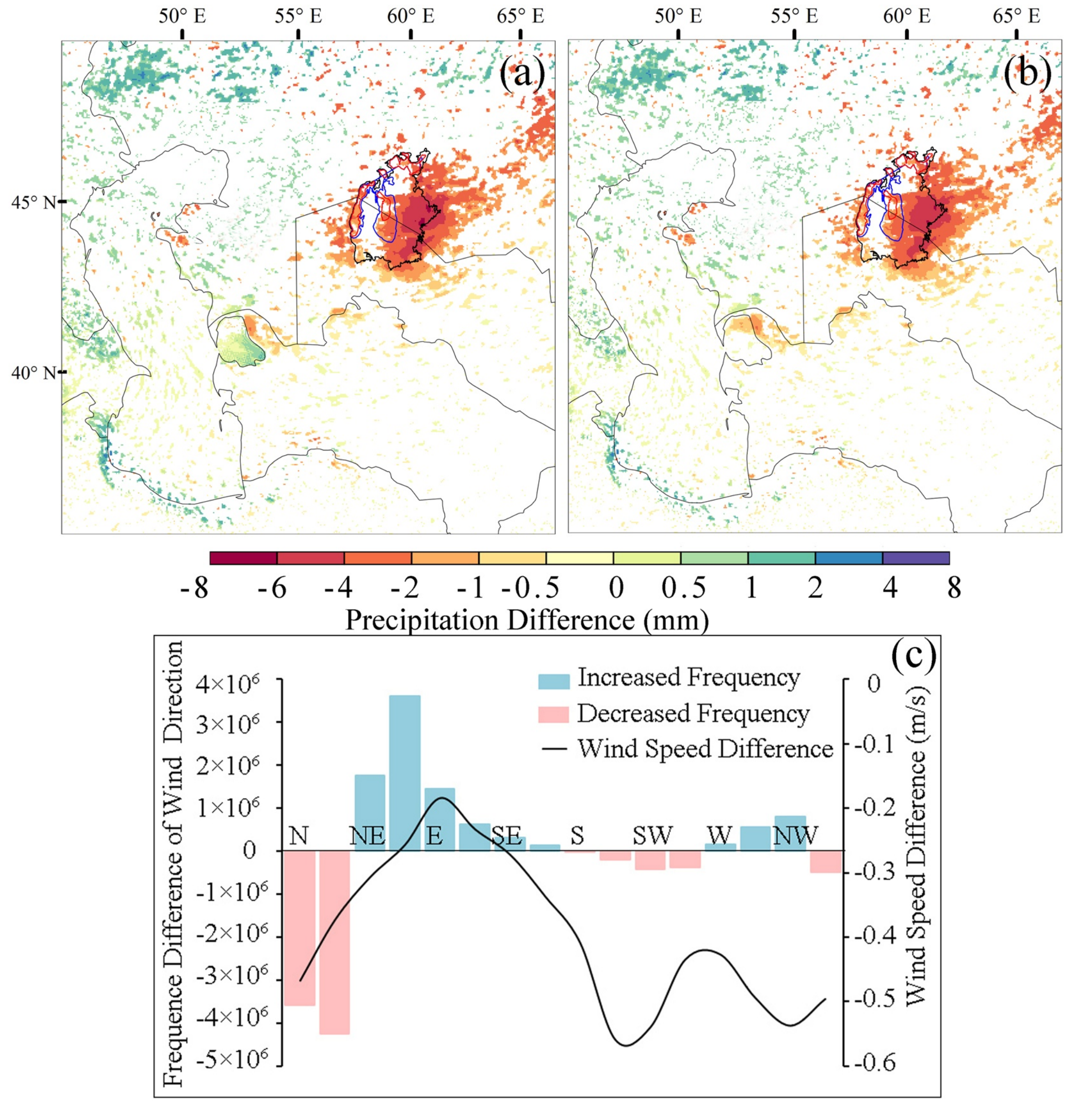

Figure 7. The spatial distribution of the total precipitation (a) and convective precipitation (b) difference computed from Case 4 to Case 3 with mean value of 36-summer. The wind direction frequency and wind speed difference (c) computed from Case 4 to Case 3 based on hourly simulation in the grids that the total precipitation significantly different between Cases 3 and 4 in eastern Aral Sea. The capital letters in (c) represent the wind direction, from left to right are north (N), north-northeast, northeast (NE), east-northeast, east (e), east-southeast, southeast (SE), south-southeast, south (S), south-southwest, southwest (SW), west-southwest, west (W), west-northwest, northwest (NW), and north-northwest, respectively.

in Figure 8c. As demonstrated in Figure 8d, the G in Case 4 is less than in Case 3 in the exposed dry bottom of the Aral Sea. But the surrounding region of the Aral Sea and western Turkmenistan demonstrates higher G in Case 4.

Concerning the domain average, LUCC induces deceasing in RN, LE, and G with amount to 1.73 W m^{-2}, 2.54 W m^{-2}, and 0.42 W m^{-2}, respectively, while the H increased by 0.87 W m^{-2}. The dry-up Aral Sea generates the most conspicuous influence, by dramatically altered the albedo which determines the amount of surface-absorbed solar energy. Hence, RN, LE, and G within the Aral Sea decreased by about 47.9 W m^{-2}, 78.67 W m^{-2}, and 23.72 W m^{-2}, respectively, while H increased by 50.19 W m^{-2}. The newly formed water surface generates opposite effects on energy fluxes and with smaller magnitudes, RN, LE, and G increased by about 22.23 W m^{-2}, 14.50 W m^{-2}, and 32.67 W m^{-2}, respectively, and reduced H by about 23.93 W m^{-2}. Other type of LUCC causes relatively smaller impacts in allocation of energy, like cropland abandoned and

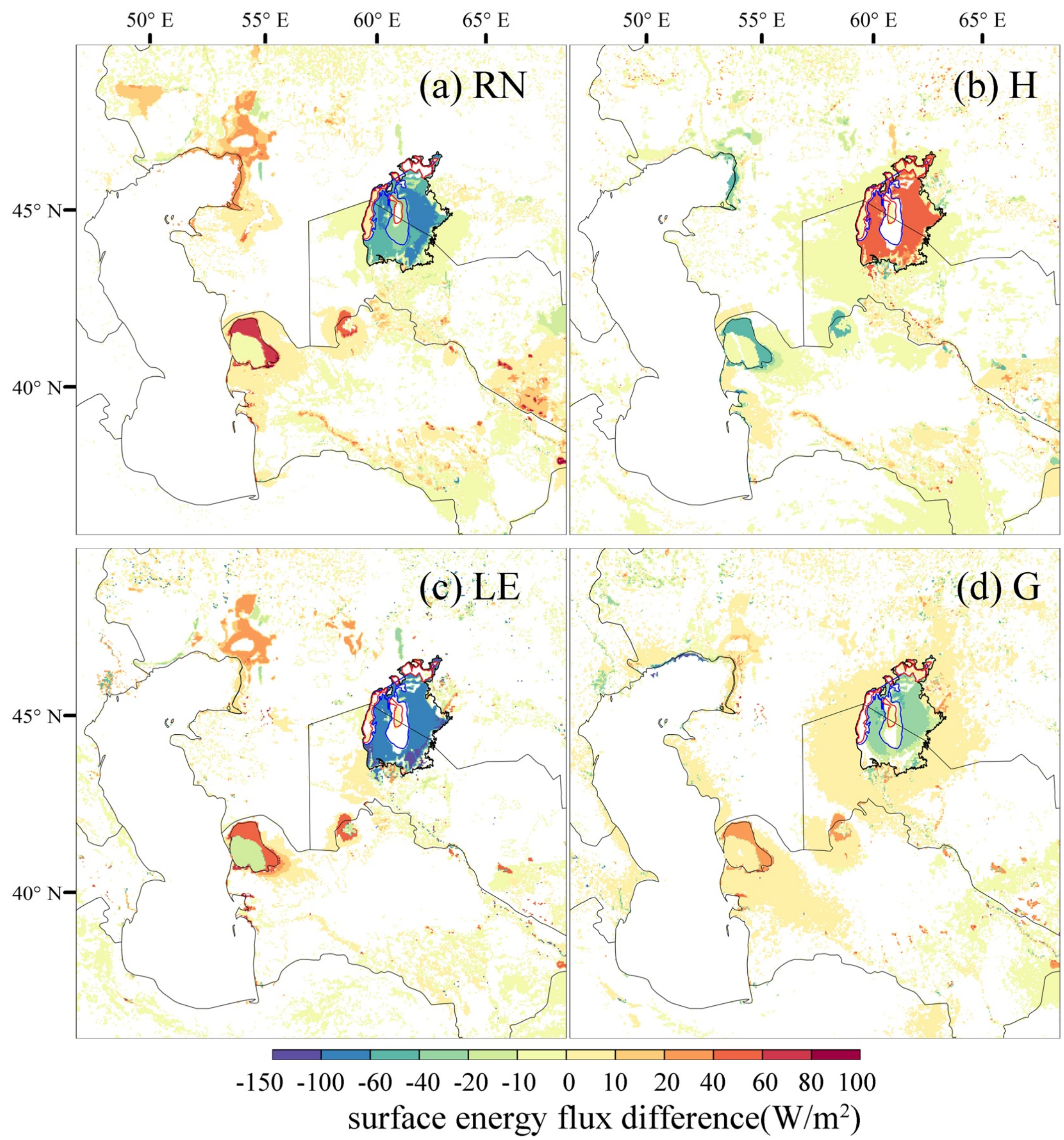

Figure 8. The spatial distribution of the surface energy fluxes differences computed from Case 4 to Case 3 with mean value of 36-summer: (a) net radiation, (b) sensible heat, (c) latent heat, and (d) ground heat flux.

grassland degeneration decreases the RN, LE, and G but increases H. Reclaimed cropland and bareland converted to grassland generates opposite influence in energy fluxes.

4. Discussion

4.1. Comparison of this Study With Prior Work

In this study, we improved the ability of the ALARO-SURFEX regional climate model to describe the regional climate by adopting more realistic land use/cover and LAI over the Aral Sea region. Though the model underestimates daily temperature and the frequency of large amount of precipitation, the error magnitudes within this study are comparable to those shown in previous downscaling studies based on regional climate models in Central Asia (Chen et al., 2019; Qiu et al., 2017; Zhang et al., 2017). We further complemented the previous studies in evaluation of the model's performance in simulating surface energy fluxes in the Aral Sea region, updated land surface parameters which showed a better ability to capture the characteristics of

10.1029/2020JD032638

hourly net radiation, sensible heat, latent heat and ground heat flux. The error magnitudes are lower than other work over the region of Central Asia (Zhang et al., 2017).

Despite the growing understanding of climate change and Aral Sea crisis, great uncertainties still exist regarding the impacts of nature and human-induced LUCC on regional climate. Due to the limitation of observed data, investigations of a long period climate change in Central Asia are mainly based on different reanalysis, interpolation, or GCMs simulation data sets. Several previous reviews (Chen et al., 2011; Hu et al., 2014; Roget & Khan, 2018) that used the reanalysis data sets (including CFSR, MERRA, ERA-Interim) and CRU to analyze the temperature change in Central Asia, both concluded that warming trend has been accelerated in the recent 40 years as shown in Table 2S of supplemental materials. The conclusions on precipitation change in Central Asia remain controversial, Chen et al. mentioned that the summer precipitation increased 2.11 mm decade^{-1} in Central Asia during late 1970s to 2009 but not significant (Chen et al., 2011), while according to 240 observations the summer precipitation decreased by 1.1 mm decade^{-1} from 1960 to 1991 but not significant (Song & Bai, 2016). It could be because the horizontal resolution of these data sets is low or most meteorological stations are distributed in the plains, which may not adequately cover the regional disparity of region's complex topography. In this study, we try to provide the climate change trend with a fine-scale spatial resolution in the recent 36 years. Our results show a stronger warming trend of T2avg (0.44°C decade^{-1}) than in the conclusions based on reanalysis data sets (0.22–0.36°C decade^{-1}). Our conclusion on summertime precipitation shows a declining trend by about −6.24 mm decade^{-1}.

Regional climate models can alleviate the deficiencies of spatial resolution to some extent. However, most researches from modeling perspective in Central Asia were focused on the impact of desiccation of Aral Sea on regional climate, with idealized experiments and limited period, which means different extents of the Aral Sea were considered while ignoring the other land cover change, summarized in Table S2 of supplemental materials. These works were based on multiple regional climate models and different horizontal resolutions. Large consensus were found in the effect of Aral Sea shrinking that led to the increase in net longwave radiation, sensible heat, near-surface temperature and diurnal temperature range, reduction in evapotranspiration, rainfall and latent heat on the dried-up Aral Sea but differences exist when concerning the magnitude and the affected area.

The impacts of the shrinking Aral Sea on summer climate have more consistent conclusions. The T2avg increasing induces by partly loss of Aral Sea in our study is 1.04°C which is in range of previous work (0–6°C) (Mcdermid & Winter 2017; Roy et al., 2014; Rubinshtein et al., 2014; Sharma et al., 2018). In terms of surface energy fluxes change caused by the desiccation of Aral Sea, our results showed net radiation reduction by 47.9 W m^{-2}, which is larger than previous work (~20 W m^{-2}). Regarding the desiccation effect of Aral Sea on summer rainfall and wind, some conclusions are partly consistent with former work. Recent work based on WRF (Sharma et al., 2018) suggested that desiccation of Aral Sea had a minor effect in precipitation and surface wind, the affected area confined in Aral Sea itself, but our results showed that the summertime rainfall (especially convective precipitation) decreased, and that the local circulation had been weaken by changing in wind direction and a decreasing in wind speed. As mentioned before, the shrinking Aral Sea increased the number of days without precipitation, which is supported by the conclusion drawn by previous work that the drought day's occurrence had risen by 300% over Aral Sea basin (Shahgedanova, 2003).

Regarding to the extent region that influenced by the shrinking Aral Sea is still controversy. Some researchers suggest the impacts of shrinking Aral Sea on temperature or precipitation are confined in the Aral Sea and vicinity region (Mcdermid & Winter 2017; Sharma et al., 2018), but some studies present conclusion that warming trend extends up to 100–200 km from the shoreline in the downwind direction (Small, Giorgi, et al., 2001). In our study, the T2avg responses to shrinking Aral Sea extends to ~400, ~310, ~170 km away on its eastern, southern and western side, respectively, the precipitation shows a further distance (approx. 400 km away). Impacts on surface energy fluxes are confined in the immediate vicinity (less than 100 km), especially latent heat flux. Other LUCC types shows slightly and small magnitude impacts on regional climate. In this study, we found that the expansion of farmland from bareland or grassland could mitigate the warming trend by 0.05°C decade^{-1}, which is consistent with Hu et al. that during 1994–2008 the warming in farmland' stations is smaller than in other stations (0.66°C versus 0.84°C) (Hu et al., 2014).

4.2. Limitations and Future Research

Our study provides the comprehensive assessment of impacts of historical LUCC on Aral Sea region with fine-scale (4 km) horizontal resolution. However, several aspects of the study can and will be improved in future work.

First, due to limitation in computation resources, our study failed to use ensemble perturbation experiments to reduce or eliminate intrinsic variability in simulations, which can obscure the subtle climate response to LUCC and possibly lead to an erroneous conclusion, especially for convective precipitation (de Elía et al., 2008; Hostetler et al., 2019; O'Brien et al., 2011). Because of the limitation in data set, our study separated the land use/cover in 3 years (1970s, 2005, and 2015). Our findings should be further confirmed by future research to consider more frequent land cover updates which can better describe actual land surface condition.

Second, because summer climate is characterized by strong interactions between the atmosphere and land surface in such arid regions. Due to the limitation of computational resources and time, we first simulated regional climate during summer. However, the impacts of desiccated Aral Sea on other season still need more efforts.

Third, in this study, we adopted the same parameters of lake depth (20 m), sediments depth (1 m), albedo (0.135), and emissivity (0.98) during the simulation period, which are inconsistent with lake in arid Central Asia. Such insufficient treatment of water bodies may influence the accuracy of model. In future work, we will pay more attention to atmosphere-water interaction and try the approach of coupled regional-lake model (Small et al., 1999, 2001b).

Finally, since the 1950s, the intensified agriculture activities and widespread use of irrigation have significant impact on the regional water-heat budget, consumed water measuring about 10,000 m^3 ha^{-1} in farmland and accordingly increasing the local evapotranspiration, which may induce the nonclosure of the surface energy balance in this region (Zhang et al., 2019). In this study, because of the limitation of observed surface energy fluxes, we only validated the model performance in natural vegetation without irrigation and further verification is needed in irrigation-intensified oasis in order to improve the model's ability in simulating fluxes (Amri et al., 2014).

5. Conclusions

This study presents the impacts of historical LUCC on regional summer climate in the Aral Sea region from a regional modeling perspective. The ALARO-SURFEX regional climate model is driven by the ERA-Interim reanalysis, at 4 km spatial resolution from 1980 to 2015.

(1) The performance of the ALARO-SURFEX improved by updating land cover and LAI. With the updated model, RMSE of T2max, T2avg, T2min, RN, H, and LE are smaller than default, the value is 3.03°C (default model is 3.16°C), 1.88 °C (2.98 °C), 1.78 °C (3.38°C), 53.52 W m^{-2} (61.63 W m^{-2}), 62.63 W m^{-2} (109.16 W m^{-2}), and 33.22 W m^{-2} (41.03 W m^{-2}), respectively. The updated ALARO-SURFEX had a better overall ability to capture the precipitation events, especially for the small magnitude precipitation.

(2) LUCC induced an increasing in T2max (0.17°C), T2avg (0.12°C), and DTR (0.10°C), but decreasing in T2min by 0.10°C. The most conspicuous difference is generated by the desiccation of Aral Sea with changes of 2.56 ± 0.88°C, 1.04 ± 0.53°C, −1.14 ± 0.56°C, and 3.42 ± 1.10°C for T2max, T2avg and T2min, and DTR, respectively.

(3) The shrinking Aral Sea caused summer precipitation decreased by 2.33 mm in the dry-up Aral Sea and approximately 400 km ribbon region in its eastern side.

(4) LUCC influenced the regional surface energy budget, causing net radiation, latent heat and ground heat to decrease by 1.73 W m^{-2}, 2.54 W m^{-2}, and 0.42 W m^{-2}, respectively, but sensible heat to increase by 0.87 W m^{-2} in domain average. Over the exposed dry bottom of Aral Sea, RN, LE, and G decreased by 47.9, 78.67, and 23.72 W m^{-2}, while H increased with an amount of 50.19 W m^{-2}.

(5) Different type of LUCC generates varying contributions to regional climate. During the period of 1980–2015, Aral Sea region shows a significant warming trend. Dried-up lake and vegetation degradation accelerated the warming trend, while the newly formed water surface and vegetation coverage increase

(reclaim cropland from grassland or bareland, conversion from bareland to grassland) slightly mitigate the warming trend.

Data Availability Statement

The ground station observations are from Global Historical Climatology Network (https://catalog.data.gov/dataset/global-historical-climatology-network-daily-ghcn-daily-version-3). The EC data used in this study is available from the corresponding author upon request. The Remote Sensing and GIS application Laboratory of Xinjiang Institute of Ecology and Geography, Chinese Academy of Sciences is gratefully acknowledged for providing the high-resolution land use/cover maps for different years, and the data is available through (Chen et al., 2015). MODIS MCD15A2H for LAI is downloaded from website of United States Geological Survey (https://lpdaac.usgs.gov/products/mcd15a2hv006/). ERA-Interim reanalysis data set is downloaded from European Center for Medium-Range Weather Forecasts Interim Reanalysis (http://apps.ecmwf.int/datasets/data/interim-full-daily/levtype=sfc). The outputs from the ALARO-SURFEX, model scripts and code for processing data in this study have been upload to Zenodo (10.5281/zenodo.4549118).

Acknowledgments
This work was jointly supported by the regional collaborative innovation project of Xinjiang (Grant No. 2020E01042), the National Natural Science Foundation of China (Grant No. U1803243), the Team project of the Chinese Academy of Sciences (Grant No. 2018-YDYLTD-002), the Open Foundation of State Key Laboratory of Desert and Oasis Ecology, Xinjiang Institute of Ecology and Geography, Chinese Academy of Sciences (G2019-02-03), the West Light Foundation of the Chinese Academy of Sciences (Grant No.2018-XBQNXZ-B-011) and China Academy of Sciences President's International Fellowship Initiative (PIFI) (Grant No. 2018VMB0006). Huili He was supported by a grant from the program of China Scholarships Council (ICPIT--International Cooperative Program for Innovative Talents, Grant No. 201804910946 201804910946) during her stay in Ghent University, Gent, Belgium.

References

Amri, R., Zribi, M., Lili-Chabaane, Z., Szczypta, C., Calvet, J. C., & Boulet, G. (2014). FAO-56 dual model combined with multi-sensor remote sensing for regional evapotranspiration estimations. *Remote Sensing*, *6*(6), 5387–5406. https://doi.org/10.3390/rs6065387

Berckmans, J., Giot, O., De Troch, R., Hamdi, R., Ceulemans, R., & Termonia, P. (2017). Reinitialized versus continuous regional climate simulations using ALARO-0 coupled to the land surface model SURFEXv5. *Geoscientific Model Development*, *10*(1), 223–238. https://doi.org/10.5194/gmd-10-223-2017

Best, M. J., Beljaars, A., Polcher, J., & Viterbo, P. (2004). A proposed structure for coupling tiled surfaces with the planetary boundary layer. *Journal of Hydrometeorology*, *5*(6), 1271–1278. https://doi.org/10.1175/JHM-382.1

Bougeault, P., & Lacarrere, P. (1989). Parameterization of orography-induced turbulence in a mesobeta-scale model. *Monthly Weather Review*, *117*(8), 1872–1890. https://doi.org/10.1175/1520-0493(1989)117<1872:POOITI>2.0.CO;2

Brovkin, V., Sitch, S., Von Bloh, W., Claussen, M., Bauer, E., & Cramer, W. (2004). Role of land cover changes for atmospheric CO_2 increase and climate change during the last 150 years. *Global Change Biology*, *10*, 1253–1266. https://doi.org/10.1111/j.1365-2486.2004.00812.x

Cai, P., Hamdi, R., He, H., Luo, G., Wang, J., Zhang, M., et al. (2020). Numerical study of the interaction between Oasis and Urban areas within an arid mountains-desert system in Xinjiang, China. *Atmosphere*, *11*(1), 85. https://doi.org/10.3390/atmos11010085

Cao, Q., Yu, D., Georgescu, M., Han, Z., & Wu, J. (2015). Impacts of land use and land cover change on regional climate: A case study in the agro-pastoral transitional zone of China. *Environmental Research Letters*, *10*(12), 124025. https://doi.org/10.1088/1748-9326/10/12/124025

Champeaux, J. L., Masson, V., & Chauvin, F. (2005). ECOCLIMAP: A global database of land surface parameters at 1 km resolution. *Meteorological Applications*, *12*(1), 29–32. https://doi.org/10.1017/S1350482705001519

Chang, Y., Hou, K., Li, X., Zhang, Y., & Chen, P. (2018). Review of land use and land cover change research progress. *IOP Conference Series: Earth and Environmental Science*, *113*, 012087. https://doi.org/10.1088/1755-1315/113/1/012087

Chen, B., & Zhou, X. (2007). Explanation of current land use condition classification for national standard of the People's Republic of China. *Journal of Natural Resources*, *22*(6), 994–1003.

Chen, F., Huang, W., Jin, L., Chen, J., & Wang, J. (2011). Spatiotemporal precipitation variations in the arid Central Asia in the context of global warming. *Science China Earth Sciences*, *54*(12), 1812–1821. https://doi.org/10.1007/s11430-011-4333-8

Chen, L., Ma, Z., & Zhao, T. (2017). Modeling and analysis of the potential impacts on regional climate due to vegetation degradation over arid and semi-arid regions of China. *Climatic Change*, *144*(3), 461–473. https://doi.org/10.1007/s10584-016-1847-2

Chen, S., Hamdi, R., Ochege, F. U., Du, H., Chen, X., Yang, W., & Zhang, C. (2019). Added value of a dynamical downscaling approach for simulating precipitation and temperature over Tianshan mountains area, Central Asia. *Journal of Geophysical Research: Atmospheres*, *124*, 11051–11069. https://doi.org/10.1029/2019JD031016

Chen, X., Bai, J., Li, X., Luo, G., Li, J., & Li, B. L. (2013). Changes in land use/land cover and ecosystem services in Central Asia during 1990-2009. *Current Opinion in Environmental Sustainability*, *5*(1), 116–127. https://doi.org/10.1016/j.cosust.2012.12.005

Chen, X., Luo, G., Wu, S., Wang, W., Hui, F., & Chen, Q. (2015). *Land use/cover change in arid land of Central Asia* (pp. 189–245). China: Science Press.

Dee, D. P., Uppala, S. M., Simmons, A. J., Berrisford, P., Poli, P., Kobayashi, S., et al. (2011). The ERA-Interim reanalysis: Configuration and performance of the data assimilation system. *Quarterly Journal of the Royal Meteorological Society*, *137*(656), 553–597. https://doi.org/10.1002/qj.828

de Elía, R., Caya, D., Côté, H., Frigon, A., Biner, S., Giguère, M., et al. (2008). Evaluation of uncertainties in the CRCM-simulated North American climate. *Climate Dynamics*, *30*(2–3), 113–132. https://doi.org/10.1007/s00382-007-0288-z

De Troch, R., Hamdi, R., Van de Vyver, H., Geleyn, J.-F., & Termonia, P. (2013). Multiscale performance of the ALARO-0 model for simulating extreme summer precipitation climatology in Belgium. *Journal of Climate*, *26*(22), 8895–8915. https://doi.org/10.1175/JCLI-D-12-00844.1

Dickinson, R. E. (1983). Land surface processes and climate—Surface albedos and energy balance. In B. Saltzman (Ed.), *Advances in geophysics* (pp. 305–353).New York: Elsevier. https://doi.org/10.1016/S0065-2687(08)60176-4

Faroux, S., Kaptué Tchuenté, A. T., Roujean, J.-L., Masson, V., Martin, E., & Le Moigne, P. (2013). ECOCLIMAP-II/Europe: A twofold database of ecosystems and surface parameters at 1 km resolution based on satellite information for use in land surface, meteorological and climate models. *Geoscientific Model Development*, *6*(2), 563–582. https://doi.org/10.5194/gmd-6-563-2013

Gaspar, P., Grégoris, Y., & Lefevre, J.-M. (1990). A simple eddy kinetic energy model for simulations of the oceanic vertical mixing: Tests at station Papa and long-term upper ocean study site. *Journal of Geophysical Research*, *95*(C9), 16179–16193. https://doi.org/10.1029/JC095iC09p16179

Gaybullaev, B., Chen, S.-C., & Kuo, Y.-M. (2012). Large-scale desiccation of the aral sea due to over-exploitation after 1960. *Journal of Mountain Science*, *9*(4), 538–546. https://doi.org/10.1007/s11629-012-2273-1

Georgescu, M., Lobell, D. B., & Field, C. B. (2011). Direct climate effects of perennial bioenergy crops in the United States. *Proceedings of the National Academy of Sciences of the United States of America*, *108*(11), 4307–4312. https://doi.org/10.1073/pnas.1008779108

Giorgi, F., & Mearns, L. O. (1999). Introduction to special section: Regional climate modeling revisited. *Journal of Geophysical Research*, *104*(D6), 6335–6352. https://doi.org/10.1029/98JD02072

Giot, O., Termonia, P., Degrauwe, D., De Troch, R., Caluwaerts, S., Smet, G., et al. (2016). Validation of the ALARO-0 model within the EURO-CORDEX framework. *Geoscientific Model Development*, *9*(3), 1143–1152. https://doi.org/10.5194/gmd-9-1143-2016

Hamdi, R., Degrauwe, D., Duerinckx, A., Cedilnik, J., Costa, V., Dalkilic, T., et al. (2014). Evaluating the performance of SURFEXv5 as a new land surface scheme for the ALADINcy36 and ALARO-0 models. *Geoscientific Model Development*, *7*(1), 23–39. https://doi.org/10.5194/gmd-7-23-2014

Hamdi, R., Van de Vyver, H., & Termonia, P. (2012). New cloud and microphysics parameterization for use in high-resolution dynamical downscaling: Application for summer extreme temperature over Belgium. *International Journal of Climatology*, *32*(13), 2051–2065. https://doi.org/10.1002/joc.2409

He, H., Luo, G., Cai, P., Hamdi, R., Termonia, P., De Maeyer, P., et al. (2021). Assessment of climate change in Central Asia from 1980 to 2100 using the Köppen-Geiger climate classification. *Atmosphere*, *12*(1), 123. https://doi.org/10.3390/atmos12010123

Heer, D. M. (1993). Geographic perspectives on Soviet Central Asia. *Population Studies*, *47*(1), 176–177. https://doi.org/10.1080/00905999308408283

Hostetler, S., Reker, R., Alder, J., Loveland, T., Willard, D., Bernhardt, C., et al. (2019). Application of a regional climate model to assess changes in the climatology of the Eastern United States and Cuba associated with historic land cover change. *Journal of Geophysical Research: Atmospheres*, *124*, 11722–11745. https://doi.org/10.1029/2019JD030965

Hu, Z., Zhang, C., Hu, Q., & Tian, H. (2014). Temperature changes in Central Asia from 1979 to 2011 based on multiple datasets. *Journal of Climate*, *27*(3), 1143–1167. https://doi.org/10.1175/JCLI-D-13-00064.1

Hua, W., & Chen, H. (2013). Recognition of climatic effects of land use/land cover change under global warming. *Chinese Science Bulletin*, *58*(31), 3852–3858. https://doi.org/10.1007/s11434-013-5902-3

Jahn, R., Blume, H. P., Asio, V. B., Spaargaren, O., & Schad, P. (2006). *Guidelines for soil description*. Rome, Italy: Food and Agriculture Organization of the United Nations.

Ji, F., Wu, Z., Huang, J., & Chassignet, E. P. (2014). Evolution of land surface air temperature trend. *Nature Climate Change*, *4*(6), 462. https://doi.org/10.1038/nclimate2223

Kabat, P., Claussen, M., Dirmeyer, P. A., Gash, J. H. C., de Guenni, L. B., Meybeck, M., et al. (2004). *Vegetation, water, humans and the climate: A new perspective on an interactive system*.Berlin: Springer Science & Business Media.

Lawrence, P. J., Feddema, J. J., Bonan, G. B., Meehl, G. A., O'Neill, B. C., Oleson, K. W., et al. (2012). Simulating the biogeochemical and biogeophysical impacts of transient land cover change and wood harvest in the Community Climate System Model (CCSM4) from 1850 to 2100. *Journal of Climate*, *25*(9), 3071–3095. https://doi.org/10.1175/JCLI-D-11-00256.1

Le Moigne, P., Boone, A., Calvet, J. C., Decharme, B., Faroux, S., Gibelin, A. L., et al. (2009). *SURFEX scientific documentation*. Paris, France: Météo-France.

Li, C., Zhang, C., Luo, G., Chen, X., Maisupova, B., Madaminov, A. A., et al. (2015). Carbon stock and its responses to climate change in Central Asia. *Global Change Biology*, *21*(5), 1951–1967. https://doi.org/10.1111/gcb.12846

Li, Z., Chen, Y., Li, W., Deng, H., & Fang, G. (2015). Potential impacts of climate change on vegetation dynamics in Central Asia. *Journal of Geophysical Research: Atmospheres*, *120*, 12345–12356. https://doi.org/10.1002/2015JD023618

Lioubimtseva, E. (2015). A multi-scale assessment of human vulnerability to climate change in the Aral Sea basin. *Environmental Earth Sciences*, *73*(2), 719–729. https://doi.org/10.1007/s12665-014-3104-1

Lioubimtseva, E., Cole, R., Adams, J. M., & Kapustin, G. (2005). Impacts of climate and land-cover changes in arid lands of Central Asia. *Journal of Arid Environments*, *62*(2), 285–308. https://doi.org/10.1016/j.jaridenv.2004.11.005

Lioubimtseva, E., & Henebry, G. M. (2009). Climate and environmental change in arid Central Asia: Impacts, vulnerability, and adaptations. *Journal of Arid Environments*, *73*(11), 963–977. https://doi.org/10.1016/j.jaridenv.2009.04.022

Masson, V. (2000). A physically-based scheme for the urban energy budget in atmospheric models. *Boundary-Layer Meteorology*, *94*(3), 357–397. https://doi.org/10.1023/A:1002463829265

Masson, V., Le Moigne, P., Martin, E., Faroux, S., Alias, A., Alkama, R., et al. (2013). The SURFEXv7.2 land and ocean surface platform for coupled or offline simulation of earth surface variables and fluxes. *Geoscientific Model Development*, *6*(4), 929–960. https://doi.org/10.5194/gmd-6-929-2013

Mcdermid, S. S., & Winter, J. (2017). Anthropogenic forcings on the climate of the Aral Sea: A regional modeling perspective. *Anthropocene*, *20*, S221330541730022X. https://doi.org/10.1016/j.ancene.2017.03.003

Meinshausen, M., Meinshausen, N., Hare, W., Raper, S. C. B., Frieler, K., Knutti, R., et al. (2009). Greenhouse-gas emission targets for limiting global warming to 2°C. *Nature*, *458*(7242), 1158–1162. https://doi.org/10.1038/nature08017

Menne, M. J., Durre, I., Vose, R. S., Gleason, B. E., & Houston, T. G. (2011). An overview of the global historical climatology network-daily database. *Journal of Atmospheric and Oceanic Technology*, *29*(7), 897–910. https://doi.org/10.1175/JTECH-D-11-00103.1

Mirzabaev, A., J. Goedecke, O. Dubovyk, U. Djanibekov, Q. B. Le, & A. Aw-Hassan, (2016), Economics of land degradation in Central Asia. In *Economics of land degradation and improvement—A global assessment for sustainable development* (pp. 261–290). Cham:Springer.

Noilhan, J., & Planton, S. (1989). A simple parameterization of land surface processes for meteorological models. *Monthly Weather Review*, *117*(3), 536–549. https://doi.org/10.1175/1520-0493(1989)117<0536:ASPOLS>2.0.CO;2

O'Brien, T. A., Sloan, L. C., & Snyder, M. A. (2011). Can ensembles of regional climate model simulations improve results from sensitivity studies?. *Climate Dynamics*, *37*(5–6), 1111–1118. https://doi.org/10.1007/s00382-010-0900-5

Ochege, F. U., Luo, G., Obeta, M. C., Owusu, G., Duulatov, E., Cao, L., & Nsengiyumva, J. B. (2019). Mapping evapotranspiration variability over a complex oasis-desert ecosystem based on automated calibration of Landsat 7 ETM+ data in SEBAL. *GIScience and Remote Sensing*, *56*(8), 1305–1332. https://doi.org/10.1080/15481603.2019.1643531

Peng, D., Zhou, T., Zhang, L., & Zou, L. (2019). Detecting human influence on the temperature changes in Central Asia. *Climate Dynamics*, *53*(7–8), 4553–4568. https://doi.org/10.1007/s00382-019-04804-2

Perkins, S. E., Pitman, A. J., Holbrook, N. J., & McAneney, J. (2007). Evaluation of the AR4 climate models' simulated daily maximum temperature, minimum temperature, and precipitation over Australia using probability density functions. *Journal of Climate*, *20*(17), 4356–4376. https://doi.org/10.1175/JCLI4253.1

Peterson, T. C., Vose, R., Schmoyer, R., & Razuvaëv, V. (2015). Global historical climatology network (GHCN) quality control of monthly temperature data. *International Journal of Climatology*, *18*(11), 1169–1179. https://doi.org/10.1002/(SICI)1097-0088(199809)18:11<1169::AID-JOC309>3.0.CO;2-U

Pielke, R. A., & Niyogi, D. (2009). *The role of landscape processes within the climate system* (pp. 67–85). Berlin: Springer.

Pielke, R. A., & Niyogi, D. (2010). The Role of Landscape Processes within the Climate System. In *Landform—Structure, evolution, process control*. Berlin:Springer.

Pielke, R. A., Pitman, A., Niyogi, D., Mahmood, R., McAlpine, C., Hossain, F., et al. (2011). Land use/land cover changes and climate: Modeling analysis and observational evidence. *WIREs Climate Change*, *2*(6), 828–850. https://doi.org/10.1002/wcc.144

Qiu, Y., Hu, Q., & Zhang, C. (2017). WRF simulation and downscaling of local climate in Central Asia. *International Journal of Climatology*, *37*(S1), 513–528. https://doi.org/10.1002/joc.5018

Roget, E., & Khan, V. M. (2018). Decadal differences of the diurnal temperature range in the Aral Sea region at the turn of the century. *Tellus A: Dynamic Meteorology and Oceanography*, *70*(1), 1–12. https://doi.org/10.1080/16000870.2018.1513290

Roy, S. B., Smith, M., Morris, L., Orlovsky, N., & Khalilov, A. (2014). Impact of the desiccation of the Aral Sea on summertime surface air temperatures. *Journal of Arid Environments*, *110*(11), 79–85. https://doi.org/10.1016/j.jaridenv.2014.06.008

Rubinshtein, K. G., Smirnova, M. M., Bychkova, V. I., Emelina, S. V., Ignatov, R. Y., Khan, V. M., et al. (2014). Studying the impact of large lake desiccation on the accuracy of numerical description of meteorological fields (a case study for the Aral Sea). *Russian Meteorology and Hydrology*, *39*(11), 727–735. https://doi.org/10.3103/S1068373914110028

Salgado, R., and P. Le Moigne, 2010, Coupling of the FLake model to the Surfex externalized surface model. *Boreal Environment Research*, *15*, 231–244

Schiemann, R., Lüthi, D., Vidale, P. L., & Schär, C. (2008). The precipitation climate of Central Asia-intercomparison of observational and numerical data sources in a remote semiarid region. *International Journal of Climatology*, *28*(3), 295–314. https://doi.org/10.1002/joc.1532

Seddon, A. W. R., Macias-Fauria, M., Long, P. R., Benz, D., & Willis, K. J. (2016). Sensitivity of global terrestrial ecosystems to climate variability. *Nature*, *531*(7593), 229–232. https://doi.org/10.1038/nature16986

Seneviratne, S. I., Corti, T., Davin, E. L., Hirschi, M., Jaeger, E. B., Lehner, I., et al. (2010). Investigating soil moisture-climate interactions in a changing climate: A review. *Earth-Science Reviews*, *99*(3), 125–161. https://doi.org/10.1016/j.earscirev.2010.02.004

Shahgedanova, M. (2003). *The physical geography of northern Eurasia*.Oxford, UK: Oxford University Press on Demand.

Sharma, A., Huang, H.-P., Zavialov, P., & Khan, V. (2018). Impact of desiccation of Aral Sea on the regional climate of Central Asia using WRF model. *Pure and Applied Geophysics*, *175*(1), 465–478. https://doi.org/10.1007/s00024-017-1675-y

Shi, H., Luo, G., Zheng, H., Chen, C., Bai, J., Liu, T., et al. (2020). Coupling the water-energy-food-ecology nexus into a Bayesian network for water resources analysis and management in the Syr Darya River basin. *Journal of Hydrology*, *581*, 124387. https://doi.org/10.1016/j.jhydrol.2019.124387

Simmons, A. J., & Burridge, D. M. (1981). An energy and angular-momentum conserving vertical finite-difference scheme and hybrid vertical coordinates. *Monthly Weather Review*, *109*(4), 758–766. https://doi.org/10.1175/1520-0493(1981)109<0758:AEAAMC>2.0.CO;2

Small, E. E., Giorgi, F., & Sloan, L. C. (1999). Regional climate model simulation of precipitation in central Asia: Mean and interannual variability. *Journal of Geophysical Research*, *104*(D6), 6563–6582. https://doi.org/10.1029/98JD02501

Small, E. E., Giorgi, F., Sloan, L. C., & Hostetler, S. (2001). The effects of desiccation and climatic change on the hydrology of the Aral Sea. *Journal of Climate*, *14*(3), 300–322. https://doi.org/10.1175/1520-0442(2001)013<0300:TEODAC>2.0.CO;2

Small, E. E., Sloan, L. C., & Nychka, D. (2001). Changes in surface air temperature caused by desiccation of the Aral Sea. *Journal of Climate*, *14*(3), 284–299. https://doi.org/10.1175/1520-0442(2001)014<0284:CISATC>2.0.CO;2

Song, S., & Bai, J. (2016). Increasing winter precipitation over arid central Asia under global warming. *Atmosphere*, *7*(10), 139. https://doi.org/10.3390/atmos7100139

Stocker, T. F., Qin, D., Plattner, G. K., Tignor, M. M. B., Allen, S. K., Boschung, J., et al. (2014). *Climate Change 2013: The physical science basis. contribution of working group I to the fifth assessment report of IPCC the intergovernmental panel on climate change*. Cambridge, UK:Cambridge University Press. https://doi.org/10.1017/CBO9781107415324

Termonia, P., Fischer, C., Bazile, E., Bouyssel, F., Brožková, R., Bénard, P., et al. (2018). The ALADIN system and its canonical model configurations AROME CY41T1 and ALARO CY40T1. *Geoscientific Model Development*, *11*, 257–281. https://doi.org/10.5194/gmd-11-257-2018

Termonia, P., Van Schaeybroeck, B., De Cruz, L., De Troch, R., Caluwaerts, S., Giot, O., et al. (2018). The CORDEX. be initiative as a foundation for climate services in Belgium. *Climate Services*, *11*, 49–61. https://doi.org/10.1016/j.cliser.2018.05.001

Turner, B. L. (1988). The earth as transformed by human action. *The Professional Geographer*, *40*(3), 340–341. https://doi.org/10.1111/j.0033-0124.1988.00340.x

Yamada, T. J., & Pokhrel, Y. (2019). Effect of human-induced land disturbance on subseasonal predictability of near-surface variables using an atmospheric general circulation model. *Atmosphere*, *10*(11), 725. https://doi.org/10.3390/atmos10110725

Yan, K., Park, T., Yan, G., Chen, C., Yang, B., Liu, Z., et al. (2016). Evaluation of MODIS LAI/FPAR product collection 6. Part 1: Consistency and improvements. *Remote Sensing*, *8*(5), 359. https://doi.org/10.3390/rs8050359

Yang, Y. U., Yuanyue, P. I., Xiang, Y. U., Zhijie, T. A., Lingxiao, S., Disse, M., et al. (2019). Climate change, water resources and sustainable development in the arid and semi-arid lands of Central Asia in the past 30 years. *Journal of Arid Land*, *11*(1), 1–14. https://doi.org/10.1007/s40333-018-0073-3

Yearbook, F. A. O. (2003). *Fishery statistics—Capture production 2001* (Vol. 92, p. 1). Rome, Italy:Food and Agriculture Organization.

Zhang, C., Lu, D., Chen, X., Zhang, Y., Maisupova, B., & Tao, Y. (2016). The spatiotemporal patterns of vegetation coverage and biomass of the temperate deserts in Central Asia and their relationships with climate controls. *Remote Sensing of Environment*, *175*, 271–281. https://doi.org/10.1016/j.rse.2016.01.002

Zhang, M., Luo, G., Cao, X., Hamdi, R., Li, T., Cai, P., et al. (2019). Numerical simulation of the irrigation effects on surface fluxes and local climate in typical mountain-oasis-desert systems in the Central Asia Arid Area. *Journal of Geophysical Research: Atmospheres*, *124*, 12485–12506. https://doi.org/10.1029/2019JD030507

Zhang, M., Luo, G., De Maeyer, P., Cai, P., & Kurban, A. (2017). Improved atmospheric modeling of the oasis-desert system in Central Asia using WRF with actual satellite products. *Remote Sensing*, *9*(12), 1273. https://doi.org/10.3390/rs9121273